# Simulation of the switching performance of an optically triggered pseudo-spark thyratron

Hoyoung Pak and Mark J. Kushner
*University of Illinois, Department of Electrical and Computer Engineering, Gaseous Electronics Laboratory, 607 East Healey, Champaign, Illinois 61820*

(Received 17 February 1989; accepted for publication 16 May 1989)

The optically triggered pseudo-spark, also known as the back-lit thyratron, is a low-pressure plasma switch having an unheated metallic cathode, which has performance specifications competitive with conventional hot cathode thyratrons. In this paper a computer simulation of the BLT is presented. The simulation consists of a $2\frac{1}{2}$-dimensional time-dependent continuum model for electron and ion transport using the local field approximation. The model includes an external circuit, and the user may specify the type of gas, pressure, geometry, and electrode materials. Predictions for the anode delay time are compared to experiment as a function of pressure ($p$), cathode-anode spacing ($d$), and trigger fluence. We find that switch closure depends critically on the formation of a virtual anode in front of the cathode hole by generation of positive space charge, and that the anode delay time decreases with increasing $p$, trigger fluence $d$, and cathode hole diameter. We also find switch performance is not well characterized by the $pd$ product as in other plasma switches. Rather, we find these quantities depend separately on $p$ and $d$ in a manner which is a function of the geometry of the cathode.

## I. INTRODUCTION

High-power plasma switches are important components in pulsed power devices including gas discharge and electron-beam-excited lasers, rail guns, and accelerators. Present and future system specifications require switches having one or more of the following characteristics: 50–100 kV holdoff, repetition rate $\leqslant$1–10 kHz, $dI/dt \geqslant 10^{12}$ A s$^{-1}$, peak current $\geqslant$30–50 kA. Hot-cathode thyratrons are presently filling many of these system requirements, however, improvements in the operating characteristics of currently available devices are still necessary to keep pace with future system requirements. A new class of plasma switches, the pseudo-spark, is currently being developed as a possible replacement for conventional hot cathode thyratrons.[1–5] The pseudo-spark is a low-pressure plasma switch which operates on the near side of Paschen's curve (increasing holdoff voltage with decreasing pressure). The pseudo-spark has demonstrated currents in excess of 10's of kA with current densities $\geqslant$10's of kA cm$^{-2}$ while using unheated metallic electrodes. The pseudo-spark, first developed in the late 1970s, was initially used as an electron and ion-beam source, and is usually electrically triggered by a trigatron device.[3,5]

The compact geometry of the pseudo-spark, though, enables construction of devices having low inductance and high $dI/dt$. These characteristics make it attractive as a high-speed switch. One variant of the pseudo-spark switch uses a cold cathode and is optically triggered by a UV light source coupled into the device using fiberoptic cables.[1,2] The device, called the back-lit thyratron (BLT), has the added advantage of not requiring heater or triggering power supplies and may therefore be electrically floated within the pulse power apparatus. The BLT is typically constructed of an inverted cup cathode having a central hole and an opposing inverted cup anode, with or without a hole (see Fig. 1). The cathode-anode separation is typically 2–5 mm and the cathode hole is typically a few mm to 1 cm in diameter. The working gas may be He, $H_2$, Ne, or Ar at pressures of 0.1–1.0 Torr. Triggering is obtained by directing photons from either an unfocused laser (directly or fiber-optically coupled) or a flashlamp onto the inside of the cup structure of the cathode. As incoherent and unfocused light may be used for triggering and auxiliary power supplies are not required, the component cost for this device may be low.

The operating characteristics of the BLT have recently been experimentally investigated by Kirkman and Gundersen,[1] Kirkman *et al.*,[2] and Hartmann *et al.*[6] They have obtained inductively limited rates of current rise of $\lesssim 10^{12}$ A s$^{-1}$ and cathode current densities in excess of 40 kA cm$^{-2}$. They have also measured electron densities during the current pulse by observing broadening of $H_\alpha$ radi-

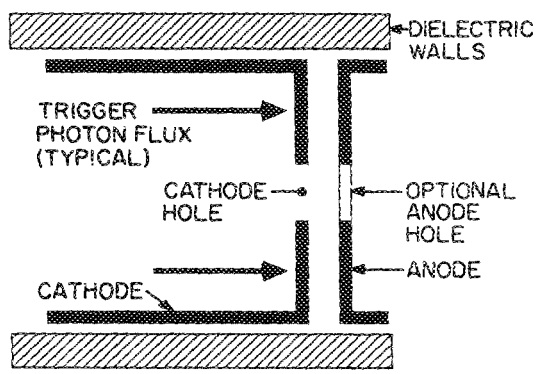


FIG. 1. A schematic of the back-lit thyratron (BLT) used in the model. The BLT consists of an inverted hollow cathode with a central hole and a plane anode. Triggering is obtained by generation of photoelectrons on the inside surface of the cathode via a photon source from either a flashlamp or laser. Critical parameters of the geometry include the anode-cathode separation and the cathode hole radius.

 0021-8979/89/182325-07$02.40  

ation.[7] In particular, the commutation characteristics (transition to a conductive state) have been investigated, including measurements of the anode delay time (delay time between optical trigger pulse and current rise) as a function of parameters such as gas pressure, and optical trigger fluence. Optically triggered pseudo-sparks, though, have not been previously theoretically analyzed or modeled.

In this paper, we report on a $2\frac{1}{2}$-dimensional time-dependent computer model with which we have studied commutation in a BLT. In this model the continuity equations for electrons and ions are solved simultaneously to solving Poisson's equation for the local electrical potential. The pertinent physical dimensions of the device, such as cathode-anode separation and cathode hold diameter, are user defined in the model, as are the gas pressure, gas composition, open-circuit voltage, and duration and amplitude of photon flux from the light source. By parameterizing the model we studied the anode delay time and switching characteristics of the BLT. We find that switch closure depends on the formation of a virtual anode in front of the cathode hole, and that the anode delay time decreases with increasing trigger photon fluence. Switching may be obtained only in a bounded region of the *p-d* (gas pressure, anode-cathode separation) plane. However, this boundary is relatively insensitive to trigger photon fluence provided that a critical minimum photon fluence is exceeded.

Our model for the back-lit thyratron is described in Sec. II. An investigation of the commutation phase of the BLT based on results from our model will be discussed in Sec. III, followed by concluding remarks in Sec. IV.

## II. DESCRIPTION OF THE MODEL

In this section we will describe our model for the back-lit thyratron (BLT). The model uses finite differences to solve the continuity equations for electrons and ions in $2\frac{1}{2}$ dimensions in either rectangular or cylindrical coordinates. The sequence of events in the simulation will first be briefly presented. As input, the user specifies the magnitude and time duration of the flux of triggering photons that are directed onto the back of the cathode. The user also specifies the gas mixture, geometry, and holdoff voltage. The simulation begins by calculating the vacuum electric field configuration and illuminating the inside of the cathode of the BLT which is holding off the voltage $V_0$. The photon flux generates secondary electrons at the surface of the cathode, which provide a source term in the electron continuity equation. The electron and ion continuity equations are then integrated in time using the local field approximation to obtain transport coefficients. The electric field is updated by solving the time-dependent form of Poisson's equations. Simultaneous to integrating the continuity equations, the flux of photons resulting from electron impact excitation of the gas and the flux of ions incident on the cathode are also computed. These fluxes, coupled with the appropriate secondary electron emission coefficients, generate a source of electrons at the cathode surface which sustains the current. The self-generated magnetic field is also computed and an effective magnetically driven drift velocity is added to the electric-field-driven drift velocity. The electron flux incident on the anode is integrated to yield the total current. Switching of the BLT and the end of commutation is denoted by a 10% decrease in voltage across the BLT while in series with a 1-Ω load. These processes are discussed in more detail below.

### A. Secondary electron emission processes

The BLT is triggered by a flux of UV photons incident on the inside of the cathode cup. We modeled the case of using a laser as the photon source. The optical pulse was 8 ns (FWHM) having an incident fluence of a few to 10's of mJ. The important parameter is, however, the product of photon flux and quantum efficiency for production of secondary electrons. The efficiency for producing photoelectrons from the materials of interest (molybdenum and nickel) are typically small. For these materials the efficiencies have been measured to be $2\times10^{-7}$ at 308 nm and $1.2\times10^{-4}$ at 222 nm.[7] Unless otherwise noted, we used a quantum efficiency of $2\times10^{-7}$.

We also included photoelectron emission due to photons generated by electron impact processes in the gas phase. We estimated that on the average, one photon is generated per ionization. The flux of photoelectrons generated by this process at position $\mathbf{r}$ on the cathode surface is therefore

$$f_e(\mathbf{r}) = \int \frac{\gamma_s n_e(\mathbf{r}') k_i[E(\mathbf{r}')N]N}{|\mathbf{r}-\mathbf{r}'|}\, d^3r', \tag{1}$$

where $n_e$ is the electron density, $N$ is the gas density, $k_i$ is the rate constant for ionization which depends on the local electric field $E$, and $\gamma_s$ is the secondary electron emission probability. Results have been obtained with and without the photoelectron emission process of Eq. (1). Switch performance, as measured by closure time, depends weakly on this contribution being at most a few percent shorter when it is included.

### B. Electric potential

The local electric potential $\phi(\mathbf{r},t)$ is obtained by solving the time-dependent form of Poisson's equation:

$$\nabla\cdot j = -\nabla\cdot\sigma\nabla\phi = -\frac{\partial\rho}{\partial t}, \tag{2}$$

where $j$ is the current density, $\sigma$ is the plasma conductivity, and $\rho$ is the charge density. Poisson's equation was solved using the method of successive over-relaxation every $10^{-11}$ $-10^{-10}$ s during the simulation. In practice, due to the sharp gradients that may occur in conductivity, we usually smoothed the conductivity using a two-dimensional digital filter before solving for the potential.

### C. Electron and ion densities

The spatially dependent electron and ion densities were obtained by integrating their respective continuity equations:

$$\frac{\partial n_e}{\partial t} = n_e N k_I + \nabla\cdot D_e\nabla n_e - \nabla\cdot v_e n_e, \tag{3}$$

$$\frac{\partial n_I}{\partial t} = n_e N k_I + \nabla\cdot D_I\nabla n_I - \nabla\cdot v_I n_I, \tag{4}$$

where $n_e$ is the electron density, $n_I$ is the ion density, $D_e$ and $D_I$ are the electron and ion diffusion coefficients, and $v_e$ and $v_I$ are the electron and ion drift velocities. These partial differential equations were reduced to ordinary differential equations using finite differences on a nonuniform mesh. The derivatives for convective transport terms were computed using the donor cell method while the diffusion terms were included using central finite differences. The ordinary differential equations obtained by these techniques, were integrated using a second-order predictor-corrector method.[8]

Transport coefficients for electrons (drift velocity, ionization coefficient, and diffusion coefficient) were obtained as a function of $E/N$ (electric field/gas number density) for $H_2$ from Ref. 9. Similarly, transport coefficients for ions were obtained from Ref. 10. Obtaining transport coefficients based on only the instantaneous local value of the electric field, or more precisely $E/N$, is the local field approximation (LFA). The LFA is quite accurate for ion transport as their equilibration distance is small compared to our scale lengths.[11] This is not necessarily true for electrons. The LFA is not strictly applicable when the energy equilibration frequency for electrons is less than the relative time rate of change of the electric field, or when the distance over which the electric field changes is small compared to the distance required for an electron to equilibrate with the field. This condition typically occurs at the higher electric fields found in the cathode-anode gap. Fortunately, little electron multiplication actually occurs in the gap, as the majority of the electrons convect into the gap from lower field regions. The LFA is therefore appropriately used. Our good systematic agreement with experimental data gives credence to the use of the LFA. As an improvement to the LFA, we have developed a multigroup (i.e., beam and bulk) description for electron transport in the BLT which will be reported on in a following publication.

### D. Magnetic-field-driven drift velocity

It is well known that high current arcs may pinch or constrict under the influence of their self-generated magnetic fields. As our interest is primarily with commutation during which currents are small, we expect that pinching will not be a dominating effect. Therefore, we may approximate its effects by use of a magnetically driven drift velocity. In this approximation, the azimuthal magnetic field $B_\theta$ is obtained by integration of the axial current density. The electrons drifting in the axial electric field experience a Lorentz force in the radial direction. By assuming that electron motion in the radial direction is mobility limited, one may compute an effective magnetically driven drift velocity, $v_r = \mu_e^2 E_z B_\theta$.[12]

## III. SIMULATION OF SWITCHING CHARACTERISTICS OF A BLT

In this section we will discuss the switching characteristics of the BLT as simulated with our model, and compare the systematic trends to experimental data. In doing so, we will point out the necessity of forming a virtual anode in the vicinity of the cathode hole in order to obtain switching.

TABLE I. Physical parameters used in the model.

| | | |
|---|---|---|
| Working gas | $H_2$ | |
| Gas pressure | 0.4 | Torr |
| Cathode-anode separation | 0.5 | cm |
| Cathode diameter | 4.4 | cm |
| Cathode hole diameter | 0.8 | cm |
| Holdoff voltage ($V_0$) | 10.0 | kV |
| Series load | 1.0 | Ω |
| Triggering photon flux | 160 | kW cm$^{-2}$ |
| Triggering photon pulse length | 8 | ns (FWHM) |

Unless otherwise noted, the conditions used for our simulation are listed in Table I. The current and voltage waveforms for this case appear in Fig. 2. Electron avalanche and the transition from commutation to conduction occurs with an anode delay time of $\approx 130$ ns. The rate of current rise during electron avalanche at commutation is $4\times 10^{11}$ A s$^{-1}$, which agrees well with experiment. As we will discuss below, the anode delay time is a function of geometry (e.g., cathode hole radius), gas pressure, trigger fluence, and holdoff voltage.

### A. Electric potential and formation of the virtual anode

Computed electric potentials within the BLT at various times during commutation are shown in Fig. 3 for the conditions of Fig. 2. In the vacuum configuration, as shown in Fig. 3(a) ($t=0$), the anode potential penetrates through the cathode hole to a value of $\approx 1$ kV. The penetration of the potential must be small in order to prevent long path breakdown extending from the inside surface of the cathode to the anode. The volume of positive potential, relative to the cathode, inside of and adjacent to the cathode hole resulting from potential penetration may be thought of as a virtual anode.

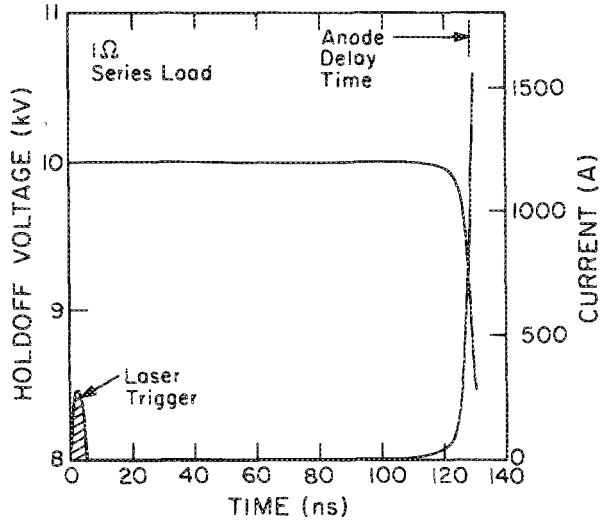


FIG. 2. Voltage and current as a function of time during the commutation phase of the BLT. The duration of the trigger photon flux is also shown. Switch closure occurs at $t\approx 120$–130 ns at which time electron avalanche becomes significant. We define the switch closure time, or anode delay time, as the time required for the voltage across the BLT to decrease by 10% of the open-circuit voltage when in series with a 1-Ω load.

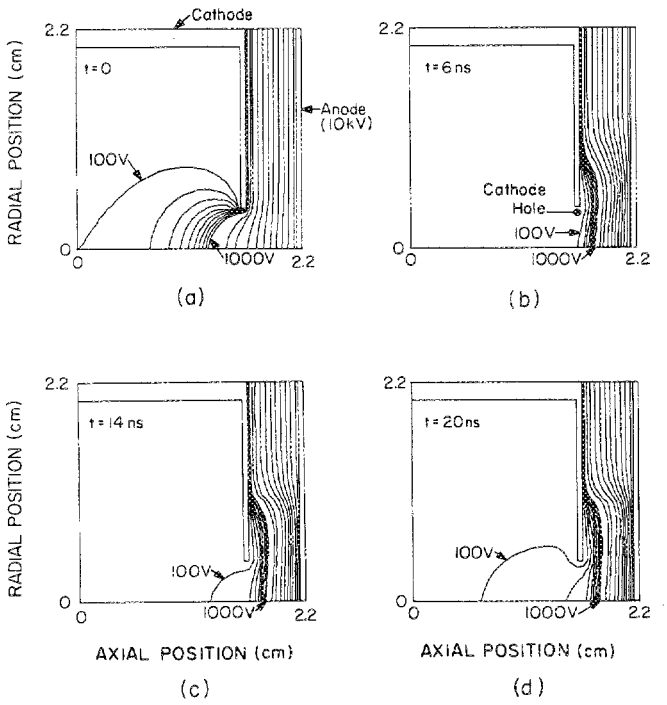


FIG. 3. Electric potential as a function of position at various time intervals. The anode potential is 10 kV. Contours are shown for 100 V increments for values $\leqslant 1$ and 1 kV intervals for $V > 1$ kV. (a) $t = 0$. The vacuum configuration is shown with penetration of the anode potential inside the cathode hole. (b) $t = 6$ ns. Negative space charge from photoelectrons cause the potential inside the cathode to recede. (c) $t = 14$ ns. Ions inside and adjacent to the cathode hole provide positive space charge, reforming the virtual anode. (d) $t = 20$ ns. The virtual anode is reformed in all instances of switch closure and is a requirement for switch closure to occur.

The virtual anode effectively increases the electric field adjacent to the cathode surface from which electrons are emitted. Although at this time this region of positive potential results from geometry rather than from space charge, as does the virtual cathode in front of a thermionic cathode, the structures are functionally equivalent.

The virtual anode survives in its vacuum configuration for only 5–6 ns after triggering. During this time, the seed photoelectrons drift away from the cathode towards the virtual anode and bring with them negative space charge which neutralizes the virtual anode. This action reduces the penetration of the anode potential through the cathode hole as shown in Fig. 3(b). If, however, this region retains a sufficiently high electric field, ionizations will occur, although at a reduced rate, adjacent to the cathode hole. The secondary electrons produced by gas phase ionizations in this region respond quickly to the electric field and pass through the cathode hole to the anode. The heavier ions, though, respond less quickly to the field and drift slowly to the cathode. The end result is that positive space charge builds up and neutralizes the negative space charge created by the photoelectrons. The virtual anode is regenerated, giving the appearance of increased penetration of the anode potential through the cathode hole as shown in Fig. 3(c). As electron avalanche proceeds the anode potential penetrates further through the cathode hole, as shown in Fig. 3(d).

In parameterizing the operating characteristics of the BLT as a function of gas pressure, electrode separation and optical trigger intensity we found that switch closure (i.e., electron avalanche and voltage collapse) occurred only when the virtual anode was regenerated in the manner described above at times $\leqslant 100$ ns after illumination of the cathode. By inference, we suggest that regeneration of the virtual anode prior to electron avalanche and voltage collapse is a requisite for switch closure.

### B. Electron density

The electron density as a function of position for various times during commutation are shown in Fig. 4 for the base case conditions. In Fig. 4(a) ($t = 4$ ns) electrons appear only near the inside surface of the cathode as they begin to avalanche after having been generated by photoemission. The electron density at this time is $\leqslant 10^9$ cm$^{-3}$. As the electrons drift towards the cathode hole [Fig. 4(b)] and into a region of higher electric field, the electron avalanche which constitutes commutation begins to intensify [Fig. 4(c)]. The onset of the conduction phase occurs approximately at 100–120 ns when the region of high electron density penetrates to the anode [Fig. 4(d)]. At this time, the electron density is $\leqslant 10^{13}$ cm$^{-3}$. Note that as the current begins to

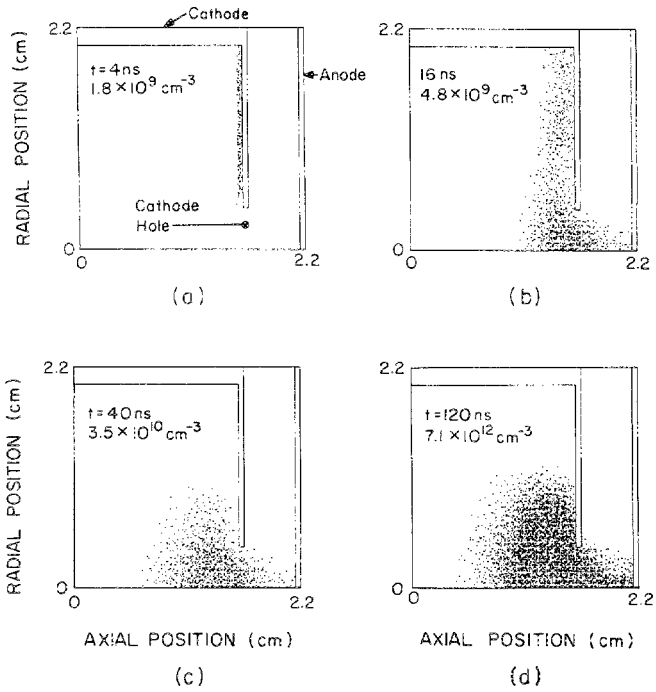


FIG. 4. Electron density as a function of position at various times after triggering. The density (cm$^{-3}$) noted in each frame is the maximum electron density at that time. (a) $t = 4$ ns. Photoelectrons are generated at the inside surface of the hollow cathode by trigger photons. (b) $t = 16$ ns. Electron motion toward the cathode hole is caused by the penetration of anode potential. (c) $t = 40$ ns. Discharge is sustained by generation of electrons due to secondary electron emission from the cathode and ionizations in the high field region. (d) $t = 120$ ns. Switch closure occurs. Note that the resolution at $t = 120$ ns has been increased by a factor of 4 to highlight the electron density in the high field region.

increase, the electrons in the cathode-anode gap actually begin to spread transversely, in agreement with experiment, as shown in Fig. 5. The radial spreading of the beam at later times results from generation of transverse components of the electric field due to negative space charge in the gap.

The volume which is deficient of electrons adjacent to the cathode is a region which resembles the cathode fall in a traditional glow discharge, somewhat misshapen due to the nonplanar geometry. As shown in Fig. 6, this region is more heavily populated by ions which provide, by bombardment of the cathode, the sustaining current for the BLT during commutation.[13,14] Secondary electrons generated by this bombardment quickly accelerate away from the cathode. Note that the region of secondary electron generation by ion bombardment, as indicated by the spatial distribution of ion density, is within a few mm of the edge of the cathode hole, which agrees well with experimental observations of the current generation area.[6] It is not clear, though, that ion bombardment alone can sustain the observed peak currents in BLTs. Hartmann *et al.*[6] suggest that field-enhanced thermionic emission may be responsible for sustaining peak current.

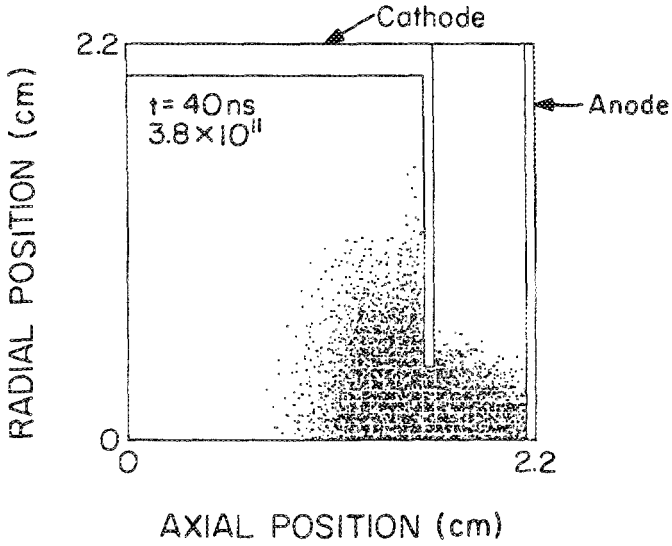


FIG. 6. Ion density as a function of position at $t = 40$ ns for conditions similar to Fig. 4. Ion bombardment of the cathode surface is necessary for sustaining of the discharge during commutation. Note that emission comes dominantly within a few mm of the cathode hole. The maximum density is $3.8 \times 10^{11}$ cm$^{-3}$ adjacent to the cathode. The resolution of the plot has been enhanced by a factor of 50 to show detail in the gap and near the cathode.

### C. Anode delay time

The switching time, or anode delay time, as a function of total photon energy (mJ) for various gas pressures is plotted in Fig. 7 for the base case conditions. The vertical surface of the cathode is uniformly illuminated. Also shown are experimental results from Gundersen *et al.*[7] Direct comparisons are difficult to make due to uncertainties in cathode coverage but we do show the same scaling. Although switching can be obtained with only 10's–100's of $\mu$J of laser energy, we have parameterized over a larger range to study the dependence of anode delay time on trigger energy. In general, if the pressure and electrode separation are in the closure regime (see below), the switching time will decrease with increasing photon fluence and decrease with increasing gas pressure. Since a critical electron density must be generated before the BLT impedance collapses, a longer avalanche time is required to reach this level when triggering with a smaller fluence. If, however, the pressure and geometry fall in the

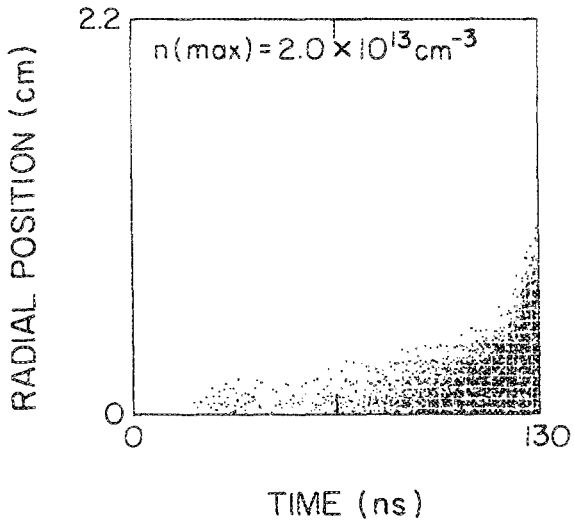


FIG. 5. Radial spreading of electron density between the anode and cathode as a function of time. The densities are for a plane 0.2 cm from the cathode. Electrons spread radially due to the generation of transverse components of the electric field.

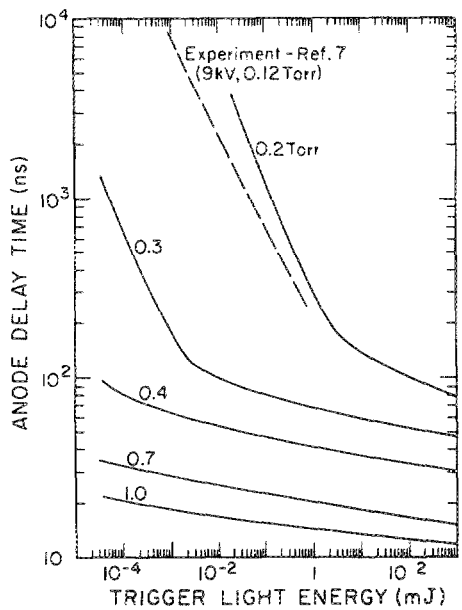


FIG. 7. Anode-delay time as a function of trigger photon energy at various gas pressures. Increasing pressure results in a shorter anode-delay time because the larger total rate of ionization offsets the reduced value of the ionization coefficient caused by the smaller $E/N$. Larger photon fluences result in shorter anode-delay times for given pressures. Experimental results are from Ref. 7 for similar representative conditions.

nonclosure regime (see below), no reasonable value of photon fluence will close the switch. We do find that there is also a critical photon fluence below which closure cannot be obtained with delay times of less than many microseconds. Due to the sensitivity of anode delay time on the incident photon fluence, we suggest that the majority of the observed jitter in this device results from shot-to-shot variations in triggering photon fluence.

The dependence of anode delay time on the diameter of the cathode hole is shown in Fig. 8. For sufficiently large cathode holes, the anode delay time is only weakly dependent on its diameter, decreasing slightly as the diameter increases. This occurs when the cathode hole diameter is significantly larger than the sheath thickness. The anode delay time increases significantly at smaller diameters until such time that closure cannot be obtained. This behavior results from reduced penetration of the anode potential through the cathode hole and overlapping of the sheaths at either side of the hole which effectively shield lower-energy electrons away.

The dependence of anode delay time on holdoff voltage is shown in Fig. 9. For holdoff voltages greater than 10 kV there is only a weak dependence of anode delay time on holdoff voltage. We expect this behavior because in hydrogen the electron transport properties (i.e., mobility and ionization coefficient) do not significantly increase in the electric fields provided by penetration of the anode potential through the cathode hole for voltages greater than $\approx 10$ kV for this geometry.

### D. Optimum switching parameters

Optimum switching conditions can be determined for a given voltage by convolving the requirements for holdoff dictated by Paschen's curve[15] (the pretrigger breakdown criterion) with the dependence of switching time on device parameters such as pressure and geometry. In order to hold

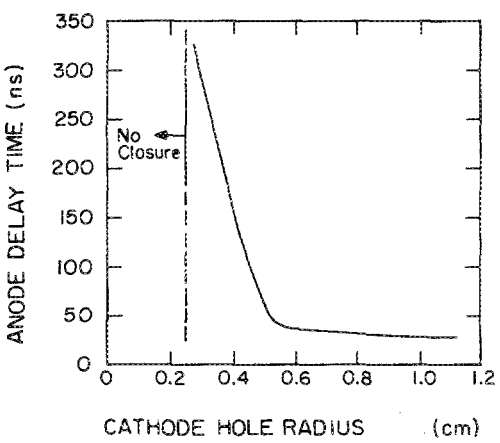


FIG. 8. Anode-delay time as a function of cathode hole radius. The dependence of anode-delay time on cathode hole radius for small cathode hole radii is a result of the lower-energy electrons being shielded away from the electrode gap by the cathode sheath. Notice that for larger values of the cathode hole radius there is only a weak dependence of anode delay time on hole radius.

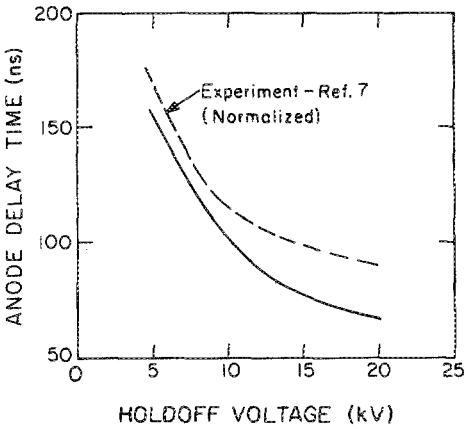


FIG. 9. Anode-delay time as a function of holdoff voltage. At values of holdoff voltage greater than 10 kV the delay time is relatively insensitive to holdoff voltage. The experimental results are from Ref. 7 and have been normalized to account for differences in trigger photon fluence.

off the desired voltage, $V_0$, one requires a combination of pressure and geometrical parameters (i.e., cathode-anode spacing) so that the *pd* product satisfies the breakdown criterion given by Paschen's curve. Since the BLT operates on the "near side" of Paschen's curve, maximum holdoff voltage increases with decreasing *pd* product. Once holdoff is obtained, one then desires to be able to trigger the device; that is, to controllably breakdown the gas by optical triggering while having a small anode delay time. The probability for post-trigger breakdown of the BLT in our geometry, and the dependence of anode delay time on pressure and electrode separation, does not simply depend on the *pd* product. Therefore, the post-trigger dependence of breakdown on pressure and electrode separation differs from the pretrigger dependence. This results from the fact that holdoff is largely determined by the ability to suppress avalanche between the two flat plates represented by the faces of the cathode and anode. The secondary electrons resulting from phototriggering, though, are emitted into an electric field which has a nonplanar geometry at the inside surface of the cathode. Also their negative space charge deforms the electric field, therefore making the electron path ill defined.

For a given value of holdoff voltage, the region where both holdoff and triggering can be obtained is bounded by two lines in the *p-d* plane as shown in Fig. 10. In this figure we show anode delay time as a function of gas pressure and cathode-anode separation. The switching time decreases with increasing gas pressure and increasing electrode separation, though not necessarily along lines of constant *pd*. The operating point of the BLT must be below a line of constant *pd* which is specified by the holdoff voltage, and above a line $f(p,d)$ which defines the region where triggering and closure will take place. At this time, $f(p,d)$ is not well represented by a line of constant *pd* and can only be specified empirically due to the complex, nonplanar geometry. Recall that the inability to trigger the BLT results, in part, from the inability of gas phase ionizations to regenerate the virtual anode in front of the cathode hole as described above. The lower boundary of this region in Fig. 10 is where the anode delay

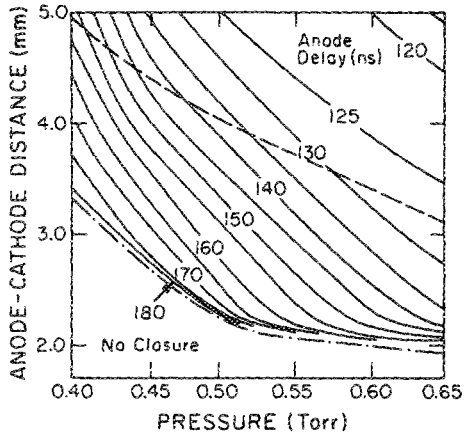


FIG. 10. Dependence of anode-delay time on gas pressure and anode-cathode separation. The delay time decreases with increasing gas pressure and decreases with larger electrode separation. The dashed line is the constant $pd$ below which satisfies Paschen's criterion at $\approx 10$ kV. The dash-dot line is $f(p,d)$ above which defines the closure region. The optimum operating points lie between these lines at values of $p$ and $d$ for which the shortest anode-delay times may be obtained.

delay times increase dramatically as a function of gas pressure or cathode-anode separation. Optimum operating conditions are those values of $p$ and $d$ below the line of constant $pd$ specified by holdoff considerations and above $f(pd)$ specified by switch closure considerations which yield the shortest anode delay time.

## IV. CONCLUDING REMARKS

A computer model for the back-lit thyratron (BLT) has been presented and its switching characteristics during commutation investigated. The commutation stage of switch closure is dominated by the secondary electron emission processes resulting from ion bombardment of the cathode and photoelectron emission from gas-phase excitation of the gas. After closure, we expect that other emission processes, such as thermal emission due to cathode heating,[16] will be necessary to obtain higher currents.

Higher gas pressures result in shorter closure times, a result of the higher collision frequency at high gas pressure resulting in a larger rate of ionization which compensates for the reduction in $E/N$. Switch closure time also decreases with increasing electrode separation, a result of an increase in the total number of electron ionizations possible over the longer path which dominates over the reduction in $E/N$. Both effects are a consequence of operating on the left-hand side of Paschen's curve. Optimum performance (faster switching speed) is therefore obtained at high gas pressures and/or large electrode separations which implies operating near the minimum of the Paschen curve. Holdoff voltage will therefore be low, thereby requiring a tradeoff between holdoff voltage and anode delay time. The fact that holdoff voltage depends on the $pd$ product while switch closure properties appear to depend more strongly on $p$ and $d$ separately enables the parameter space for the tradeoff to be larger than perhaps in conventional thyratrons.

For a given $p$ and $d$, the anode delay time also depends upon the fluence of the trigger photons for short ( $< 10$'s of ns) optical pulses. Gas pressure and electrode separation determine whether or not the switch is able to close provided that some minimum triggering photon fluence is used. Above this value the photon fluence determines the speed of switch closure, and the anode delay time decreases with increasing photon fluence. In the nonclosure regimes, increasing the photon fluence will not cause closure. Under these conditions closure is prevented by the fact that the virtual anode in front of the cathode hole is not reformed after being neutralized by the negative space charge of the photoelectrons. Regeneration of the virtual anode requires a critical amount of gas-phase ionization, which is a condition ultimately determined by geometry and local $E/N$ as opposed to photon fluence.

## ACKNOWLEDGMENTS

This work was supported by Los Alamos National Laboratory under the direction of Dr. Glen McDuff. We acknowledge and thank Dr. Martin Gundersen of the University of Southern California for his valuable advice and access to his experimental data prior to publication.

[1] G. Kirkman and M. Gundersen, Appl. Phys. Lett. **49**, 494 (1986).
[2] G. Kirkman, W. Hartmann, and M. Gundersen, Appl. Phys. Lett. **52**, 613 (1988).
[3] K. Frank, E. Boggasch, J. Christiansen, A. Goertler, W. Hartmann, C. Kozlik, G. Kirkman, C. Braun, V. Dominic, M. Gundersen, H. Riege, and G. Mechtersheimer, IEEE Trans. Plasma Sci. **PS-16**, 317 (1988).
[4] G. Mechtersheimer, R. Kohler, T. Lasser, and R. Meyer, J. Phys. E **19**, 466 (1986).
[5] D. Bloess, I. Kamber, H. Riege, G. Bittner, V. Brueckner, J. Christiansen, K. Frank, W. Hartmann, N. Lieser, C. Scheitheiss, R. Seeboeck, and W. Seudtner, Nucl. Instrum. Methods **205**, 173 (1983).
[6] W. Hartmann, V. Dominic, G. Kirkman, and M. Gundersen, Appl. Phys. Lett. **53**, 1699 (1988).
[7] M. Gundersen (unpublished).
[8] M. Abramowitz and I. Stegun, *Handbook of Mathematical Functions*, (Dover, New York, 1972), pp. 896–897.
[9] J. Dutton, J. Phys. Chem. Ref. Data **4** (1975).
[10] H. Ellis, R. Pai, E. McDaniel, E. Mason, and L. Viehland, At. Data Nucl. Data Tables **17**, 177 (1976).
[11] J. E. Lawler, Phys. Rev. A **32**, 2977 (1985).
[12] M. J. Kushner, R. D. Milroy, and W. D. Kimura, J. Appl. Phys. **58**, 2988 (1985).
[13] B. Chapman, *Glow-Discharge Processes* (Wiley, New York, 1980), pp. 82–95.
[14] B. Szapiro, J. Rocca, and T. Prabhuram, Appl. Phys. Lett. **53**, 358 (1988).
[15] J. Cobine, *Gaseous Conductors* (Dover, New York, 1958), pp. 162–168.
[16] C. Braun, V. Dominic, G. Kirkman, W. Hartmann, M. Gundersen, and G. McDuff, IEEE Trans. Electron Devices **ED-35**, 559 (1988).